Self-Assembly of Extended Polycyclic Aromatic Hydrocarbons on Cu(111)

Pascal Ruffieux,*,† Oliver Gröning,† Roman Fasel,† Marcel Kastler,‡ Daniel Wasserfallen,‡ Klaus Müllen,‡ and Pierangelo Gröning†

Empa, Swiss Federal Laboratories for Materials Testing and Research, Feuerwerkerstrasse 39, 3602 Thun, Switzerland, and MPI for Polymer Research, Ackermannweg 10, 55128 Mainz, Germany

Received: December 8, 2005; In Final Form: March 24, 2006

We present a low-temperature scanning tunneling microscopy study on the self-assembly of extended polycyclic aromatic hydrocarbons with different symmetries on the Cu(111) surface. All molecules show a commensurate monolayer structure, with significant structural differences with respect to the unit cell of the molecular lattice and the orientational ordering. We find that the molecular lattice and the molecular orientation are largely dominated by molecule−substrate interactions, whereas molecule−molecule interactions determine the molecular packing density via steric repulsion. Moreover, we show that the structure of the monolayer is transferred to the second layer via molecule−molecule interaction.

Introduction

The aim to build functional molecular structures by self-assembly has recently driven a considerably large number of investigations for structures in solution as well as at surfaces.[1] Regarding self-assembly at surfaces, basic requirements are the preparation of substrate surfaces acting as appropriate templates for molecular structures and the design of molecules incorporating functional groups on a molecular core having adequate properties regarding adsorption at predefined positions on the surface. Considerable progress has been achieved in the design of surface structures that might serve as nucleation templates on the nanometer scale by using surface reconstruction patterns,[2] strain-relief patterns,[3,4] structures evolving from lattice mismatch,[5] and vicinal surfaces.[6] However, the application of such template structures for the controlled positioning of molecular building blocks remains to be demonstrated. Furthermore, the structure of supramolecular aggregates can be controlled by exploiting selective and directional noncovalent interactions between molecules. Recently, such concepts have been used to stabilize two-dimensional structures by using hydrogen bonding,[7,8] dipolar coupling,[2,1] or metal coordination.[9]

Polycyclic aromatic hydrocarbons (PAHs) based on the structure of hexa-*peri*-hexabenzocoronene (HBC, $C_{42}H_{18}$) show a large structural variety offering the possibility to accommodate functional groups with different symmetries.[10] The large aromatic core of the molecule acts as an electron reservoir, motivating the application of HBC-based molecules as building blocks for molecular electronics. Recent studies showed the possibility of controlling the charge state of the core by attaching charge-transfer complexes to the HBC molecule, allowing the building of a prototypical single-molecule chemical-field-effect transistor.[11]

Previous investigations of the self-assembly of PAHs revealed commensurate structures with the substrate, indicating a rather strong interaction with the surface atom layer.[12−14] For HBC it has been shown that the $\pi-\pi$ interaction between the cores determines the growth mode perpendicular to the aromatic core, favoring the growth of one-dimensional columnar structures in solution,[15,16] as well as for vacuum preparation at metal surfaces.[17]

To investigate the role of core geometry on the monolayer and stacking behavior we have investigated three different PAHs with small structural differences that change the contour and symmetry of the molecules. The molecules are hexa-*peri*-hexabenzocoronene (HBC, $C_{42}H_{18}$), dibenzo[*hi*,*uv*]phenanthro-[3,4,5,6-*b*,*c*,*d*,*e*,*f*]ovalene (DPO, $C_{46}H_{18}$) and dibenzo[*fg*,*ij*]-phenanthro[9,10,1,2,3-*p*,*q*,*r*,*s*,*t*]pentaphene (DBPP, $C_{36}H_{18}$) with 6-fold, 2-fold, and 1-fold symmetry, respectively (Figure 1).

Experimental Section

Experiments were performed in an ultrahigh-vacuum chamber with a low-temperature scanning tunneling microscope (STM).[18] The Cu(111) surface was prepared by several cycles of Ar^+ ion sputtering and subsequent annealing to 800 K. The synthesis of HBC and DBPP is described elsewhere.[19,20] For the DPO molecule synthesis details are provided in the Supporting Information. Monolayer systems were prepared by vacuum sublimation from heated quartz crucibles (Kentax, TCE-BSC) with the sample kept at room temperature. A quartz microbalance was used for thickness calibration. Evaporation temperatures were chosen to complete a monolayer in ∼7 min, followed by annealing of the sample to ∼500 K to allow molecular diffusion for the formation of well-ordered monolayer structures. Subsequently, the sample was cooled to 77 K directly in the STM.

Results and Discussion

Monolayer Structure of HBC. STM images of a monolayer of HBC on Cu(111) reveal a hexagonal arrangement of the molecules with a nearest-neighbor (NN) distance of 14.2(1) Å (Figure 2). This is in excellent agreement with the NN distance of 14.2 Å determined from low-energy electron diffraction (LEED) where the pattern can be directly related to a $(\sqrt{31} \times \sqrt{31})R \pm 8.95°(\sqrt{31})$ superstructure with respect to the Cu(111) surface unit cell. Furthermore, the hexagonal molecular

* Address correspondence to this author:. Phone: +41-33-228-2296. Fax: +41- 33-228-4490. E-mail: pascal.ruffieux@empa.ch.
† Empa, Swiss Federal Laboratories for Materials Testing and Research.
‡ MPI for Polymer Research.

10.1021/jp057158w CCC: $33.50
Published on Web 05/24/2006

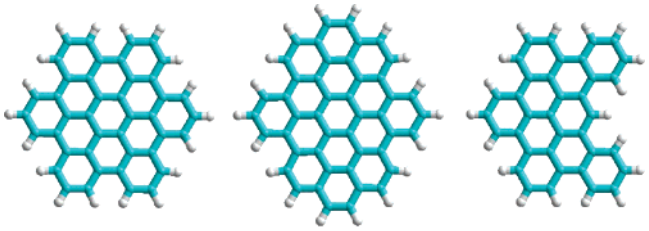

Figure 1. Structure of (**1**) hexa-*peri*-hexabenzocoronene (HBC, $C_{42}H_{18}$), (**2**) dibenzo[*hi*,*uv*]phenanthro[3,4,5,6-*b*,*c*,*d*,*e*,*f*]ovalene (DPO, $C_{46}H_{18}$), and (**3**) dibenzo[*fg*,*ij*]phenanthro[9,10,1,2,3-*p*,*q*,*r*,*s*,*t*]pentaphene (DBPP, $C_{36}H_{18}$).

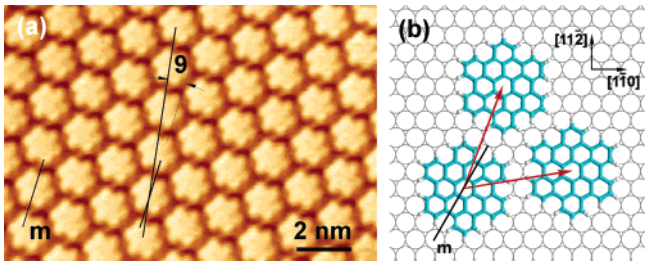

Figure 2. Monolayer structure of HBC on Cu(111): (a) STM image ($U = 5$ mV, $I = 0.03$ nA). The molecular axis *m* is indicated. (b) Proposed molecular orientation and $(\sqrt{31} \times \sqrt{31})R \pm 8.95°$ superstructure.

shape resolved by STM allows the determination of molecular orientation. Comparison of the molecular orientation and NN directions reveals that the orientation in the monolayer structure deviates from the one expected for a close-packed structure of hexagonal molecules, in the way that the molecular axis *m* of the molecule is rotated by ~9° with respect to the nearest-neighbor (NN) direction. Comparison with the structure of the Cu surface lattice shows that the molecular axis *m* is parallel to the direction of the close-packed Cu atom rows, which is in agreement with results from a previous X-ray photoelectron diffraction study.[17] This orientation is apparently stabilized by the alignment of the Cu atom rows and the carbon rings of the molecule due to the nearly identical separations between Cu atoms ($d_{Cu} = 2.55$ Å) and the benzene rings (2.5 Å). The same orientation is found for isolated single molecules adsorbed on the Cu(111) surface,[21] where the lock into registry of the molecule with the Cu lattice is observed during lateral manipulation with the STM tip. These observations evidence a molecule−substrate interaction that is strongly modulated with the periodicity of the Cu atom lattice and explain the growth of commensurate superstructures for the HBC monolayer on the Cu(111) surface. Accordingly, the observed monolayer structure with the molecules rotated by 9° with respect to the NN direction results in the densest possible commensurate packing with the carbon rings oriented along the direction of close-packed Cu atom rows.

Submonolayer Structure of HBC. Deviations from the above-described behavior are observed on terraces where the molecule density is too low for completing a close-packed monolayer. Figure 3a shows a STM image of such a terrace, where two domains with different molecular lattices and densities can be observed. The domain labeled *A* has the usual structure of a close-packed HBC monolayer, whereas domain *B* has a molecular lattice that differs from this structure. The Fourier transformed STM image (Figure 3b) reveals the characteristic differences between the two domains with two different sets of wave vectors describing the molecular lattices

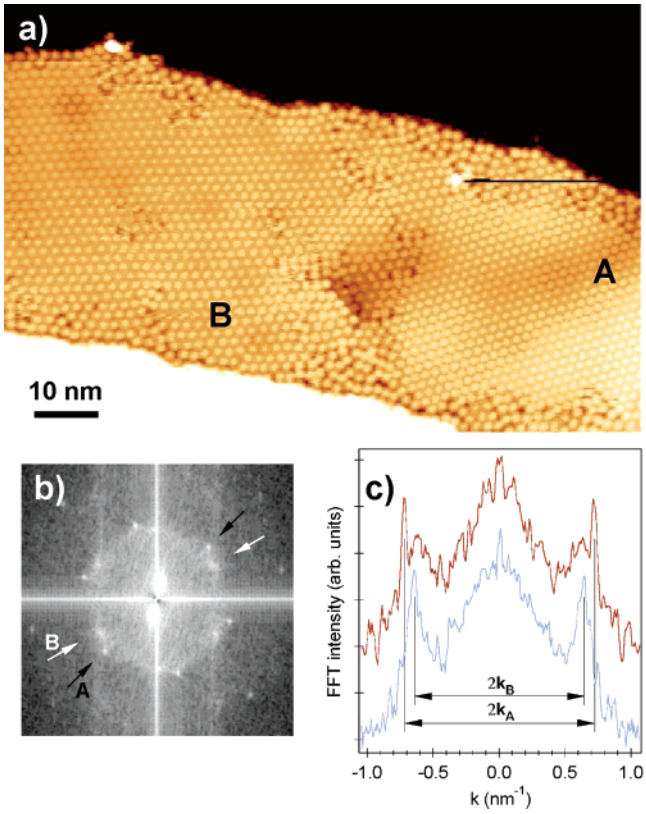

Figure 3. Submonolayer structure of HBC on Cu(111). (a) STM image showing a saturated monolayer domain (*A*) coexisting with a lower density phase (*B*) on the same terrace ($U = 2.2$ V, $I = 0.04$ nA). (b) Corresponding FFT image of the STM image shown in part a. (c) Line profiles of the FFT image shown in part b at positions marked by arrows.

in domains *A* and *B*. According to the difference of the wave vectors we deduce a NN molecule separation enhanced by ~11% and a rotation of the NN direction of 15° for domain *B* compared to the close-packed monolayer *A*. The observed lattice is in agreement with a $(\sqrt{37} \times \sqrt{37})R \pm 25.3°(\sqrt{37})$ superstructure, which compares to the dense monolayer structure with an increase of the NN molecule distance of 9.3% and a relative angle of 16.3°.

This result is in agreement with investigations at very low molecule coverage,[21] showing that island formation is completely suppressed for HBC molecules although molecular mobility at room temperature is rather high. The above-mentioned observations suggest that the $\sqrt{31}$-structure only appears when the first monolayer is completely saturated. At lower coverage a lattice with larger NN separations is energetically more favorable than partial filling of the terrace with the saturated monolayer structure. Hence, the molecule−molecule interaction within the first HBC layer is repulsive on Cu(111), which is in contrast to a small attractive van der Waals-related interaction that is expected for free molecules.

The different adsorption properties of the molecules in the two domains also become visible when scanning with different parameters. Whereas the densely packed $\sqrt{31}$-domain *A* is stable for a very broad sample bias window (ca. −2 to ca. 2 V), the molecules in the $\sqrt{37}$-domain *B* are destabilized when scanning with negative bias. STM images taken with these tunneling parameters inhibit the resolution of the molecular lattice in domain *B* due to a largely suppressed corrugation. However, the apparent height of the molecules is identical with that of the stable molecules in domain *A*. This observation seems

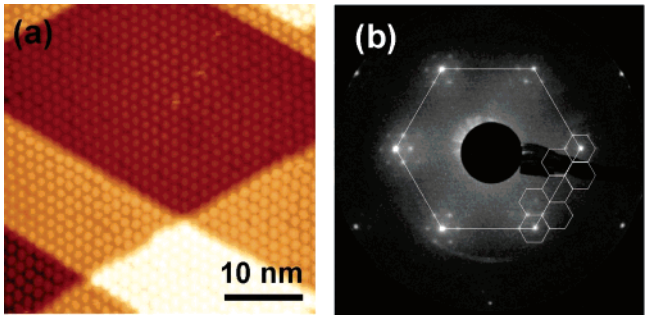

Figure 4. DPO monolayer structure on Cu(111): (a) STM image ($U = 0.1$ V, $I = 0.05$ nA) and (b) LEED, 186 eV at 150 K.

to be directly related to the less dense packing in domain *B*. The attractive interaction with the scanned tip might then pull the molecules out of their equilibrium position, resulting in a corrugation-less image. This is confirmed by Scanning Tunneling Spectroscopy, which shows an increased tunneling resistance for negative bias, i.e., for a given current setpoint the tip is closer at the surface for negative bias. This tip-induced mobility seems to be largely suppressed in the denser domain *A*. This is further corroborated by calculations of the nonbonded interactions between two neighboring molecules where we find an equilibrium distance of 14.1 Å.[17] The NN distance of 14.2 Å in domain *A* is thus very near the equilibrium distance and pulling the molecules away from this position directly results in a repulsive contribution from the neighboring molecules, which further stabilizes the molecule during scanning.

Monolayer Structure of DPO. Compared to HBC, the DPO molecule has a lower rotational symmetry (C2) due to the four additional carbon atoms in the aromatic core. This leads to two additional carbon rings along the long axis of the molecule. In Figure 4 we show an STM overview image and a LEED pattern of the close-packed monolayer structure of DPO on Cu(111). The LEED pattern reveals a commensurate (6 × 6) structure with respect to the Cu(111) lattice. The corresponding NN molecule separation is 15.3 Å. From STM images we determine an average NN molecule separation of 15.4 Å, in good agreement with the diffraction experiment.

High-resolution STM images of the 6 × 6 structure reveal further details about the orientation of the DPO molecules, as shown in Figure 5. We find three possible molecular orientations with respect to the Cu lattice. The arrangement of the differently orientated molecules results in a $\begin{pmatrix} 2 & -1 \\ 0 & 4 \end{pmatrix}$ superstructure with respect to the (6 × 6) lattice discussed above. According to the symmetry of the Cu(111) surface three orientations of the superstructure unit cell are possible, and for each of them two equivalent domains with a mirror axis along the close-packed rows of the Cu atoms are possible. The superstructure is also resolved in the Fast Fourier Transform (FFT) of the STM image (Figure 5b). Intensity maxima related to this superstructure are highlighted by open squares.

Despite the small structural difference of the DPO with respect to HBC the self-ordering at the surface is fundamentally different. The slightly larger size inhibits the arrangement in the same commensurate superstructure as HBC due to repulsive intermolecular forces along the long axis. Accordingly, the average NN separation is significantly increased. Compared to HBC, we find an increase of ~8% as determined from LEED and STM measurements. Due to the lower symmetry, different nonequivalent orientations of the molecule exist at the surface. However, we only observe orientations where neighboring carbon rings are aligned with the Cu atom rows, i.e., only three orientations are identified. This indicates that also in the case

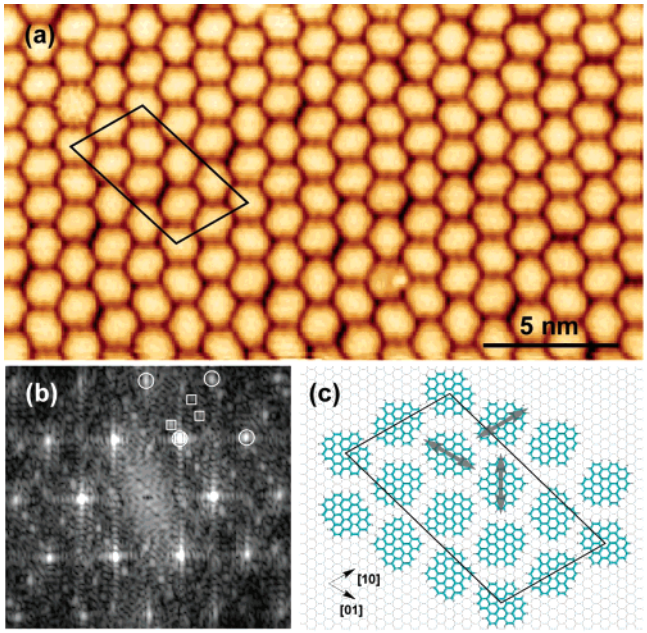

Figure 5. Local structure of DPO on Cu(111). (a) High-resolution STM image ($U = -1.5$ V, $I = 0.05$ nA). (b) Calculated FFT image of part a. Circles highlight the spots originating from quasihexagonal arrangement of the molecules. Squares highlight spots related to the orientational superstructure. (c) Proposed unit cell structure.

of DPO the molecule−substrate interaction plays a key role in the self-ordering of the monolayer film. The molecular superstructure observed in STM images reveals a unit cell containing all three nonequivalent molecular orientations. However, for a given domain the monolayer structure does not show a uniform occupation of the three possible molecular orientations. Four of the molecules in the superstructure unit cell are oriented with the molecular axis *m* along the short lattice vector of the superstructure unit cell. The remaining molecules have orientations in the other two allowed directions with two molecules for each direction. According to these observations we propose a molecular arrangement as shown in Figure 5c. The model accounts for the orientations observed with STM and the average NN separation of 6 d_{Cu} on Cu(111). With respect to the Cu lattice this superstructure is described by a $\begin{pmatrix} 24 & -6 \\ 0 & 12 \end{pmatrix}$ unit cell. Despite the large size of the unit cell (containing 288 Cu atoms), only a few defects in molecular ordering are observed.

Monolayer Structure of DBPP. Figure 6 shows an overview STM image of approximately 1.3 monolayers of DBPP on Cu(111). Excess molecules that cannot be incorporated in the first monolayer aggregate to small islands in the second monolayer. The FFT of the STM image (inset) reveals a hexagonal lattice that dominates the long-range order of the molecules. The two visible sets of hexagonal spots can be attributed to the molecular lattices of the lowest terrace in the upper part of the image and the two higher terraces in the lower part, respectively. A small fraction of the molecules form structures that deviate from the hexagonal lattice. These molecules are arranged in a double-row structure with a different NN direction, as will be described later.

LEED analysis of the same sample reveals a diffraction pattern that shows the same symmetry as the FFT image. From the LEED patterns we deduce a $(\sqrt{31} \times \sqrt{31})R \pm 8.95°$ superstructure, i.e., the same superstructure as for HBC. Higher resolution STM images reveal the arrowlike asymmetric shape of the DBPP molecule, showing a part of a hexagon with four resolved sides and a missing corner (Figure 7a). We observe a

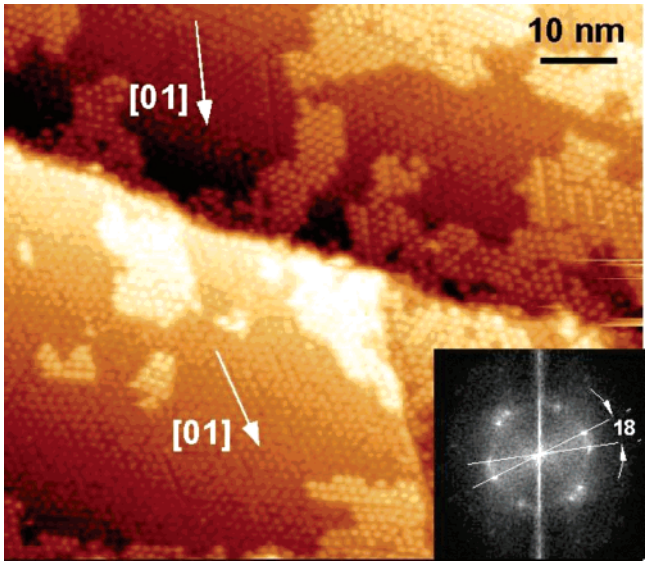

Figure 6. Overview STM image ($U = 0.4$ V, $I = 0.001$ nA) of 1.2 ML of DBPP on Cu(111). The calculated FFT image shown in the inset reflects the superposition of two hexagonal lattices that are rotated by 18° with respect to each other.

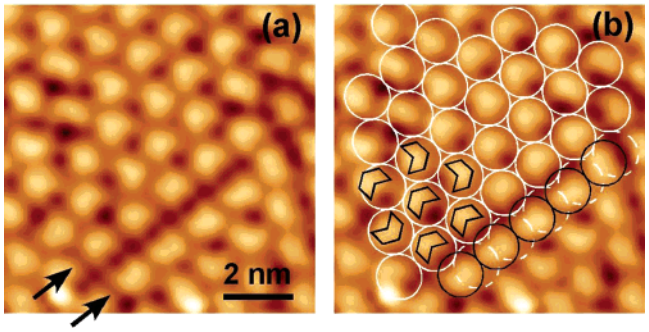

Figure 7. (a) High-resolution STM image ($U = 0.4$ V, $I = 0.001$ nA) of the monolayer structure of DBPP on Cu(111). Arrows indicate molecules arranged in the double-row structure. (b) Same image as in part a with arrows indicating the orientation of the molecules. White circles indicate molecule positions corresponding to a hexagonal ordering. Black circles indicate the molecule positions in the double-row structure.

stochastic distribution of six different orientations of the molecule within the hexagonal lattice. The position of the molecules, however, accurately follows the hexagonal lattice defined by the $\sqrt{31}$-superstructure, as shown in Figure 7b.

Whereas most molecules are arranged in a hexagonal lattice there also exist aggregates with a different symmetry. These aggregates consist of a double row of molecules where all molecules in a row are equally oriented with the arrow pointing away from the opposite row. The double-row structures have a typical length of 4−6 molecules. The molecules within a row have the same nearest-neighbor directions and distances as the hexagonally arranged molecules characterized by the $\sqrt{31}$-superstructure. However, the nearest molecule in the opposite row deviates from the superstructure lattice in terms of the NN direction as well as the NN distance, which is shorter by about 20%.

Comparison of the apparent arrowlike shape of DBPP with STM images of HBC allows a direct identification of the missing corner (the back of the arrow) with the missing carbon ring compared to the HBC structure. Accordingly, the molecules have again the same six allowed orientations on Cu(111) with the carbon rings being aligned with the Cu atom rows. The

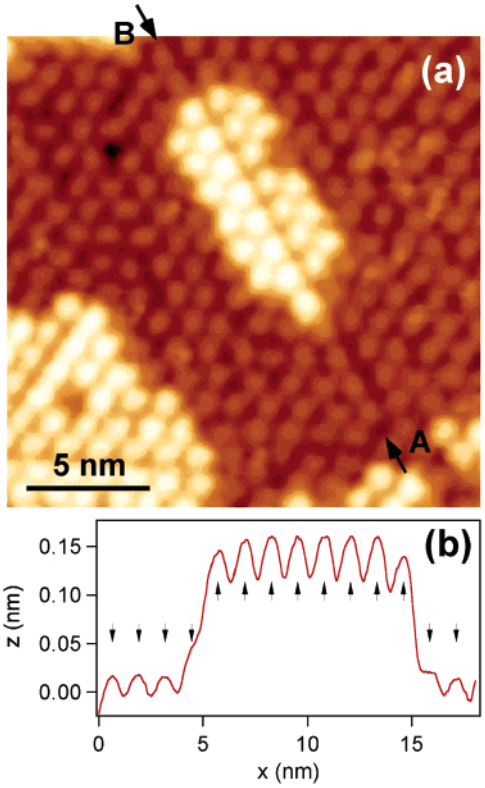

Figure 8. (a) STM measurement of DBPP clusters in the second layer ($U = 0.4$ V, $I = 0.001$ nA). (b) Line profile along the double-row structure from position *A* to position *B* marked in part a. Arrows pointing downward mark the positions of the first layer molecules. Arrows pointing upward indicate positions according to the continued sequence of the first layer molecule positions.

observed self-ordering of the DBPP molecules is surprising with regard to the molecular lattice, which is identical with that of the larger HBC molecules. Although a small fraction is arranged in the denser double-row structure, there is no long-range phase that evolves from these local structures. The limited size of these structures can be understood when taking a closer look at the molecular configuration in the rows. Since the molecules within a row are all equally oriented with the arrow pointing away from the opposite row, they define an outer periphery that is exactly the same as that of a row of HBC molecules. Therefore, the periphery nucleates the growth of a hexagonal lattice if there is no significant adsorption energy difference for neighboring molecules with different orientations. This seems to be the case for the DBPP molecule since no preferential orientational ordering is found in the hexagonal lattice.

Transfer of Structural Information to the Second Layer of DBPP. Figure 8 shows a region with small DBPP clusters in the second monolayer. The underlying molecules form an elongated double-row cluster, as discussed above. Examining the line profile shown in Figure 8b, we find that the molecule position of the double-row sequence in the first monolayer is transferred to the second layer. This can be seen by comparing the set of arrows marking the continued molecule sequence of the first layer and the profile maxima originating from molecules of the second layer. However, not only the molecule position is transmitted to the second layer but also the molecular orientation. As for the double-row structure in the first monolayer the arrow-shaped molecules in the second layer point away from the opposite molecule row.

The structure transmitted from the first to the second monolayer shows that the potential landscape relevant for

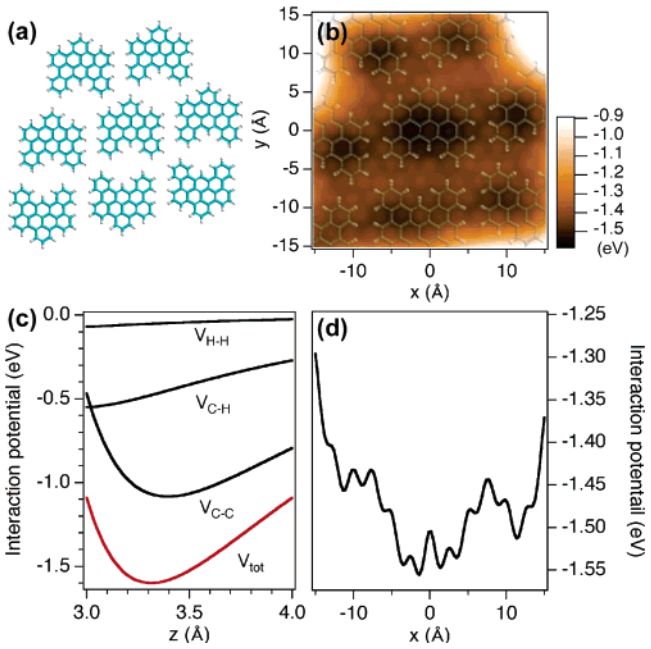

Figure 9. Intermolecular potential between a molecule in the second layer and the monolayer structure. (a) Cluster of 8 molecules used as a model for the double-row structure in the first layer. (b) Potential landscape for a molecule in the second layer. The shifts in *x* and *y* are with respect to the center molecule in part a. Positions of the molecules in the first layer are indicated. (c) Interaction potential as a function of the height *z* of the molecule with respect to the first layer. (d) Line profile of the potential landscape shown in part b at $y = 0$.

molecules adsorbed in the second layer has specific minima, which are related to the position of molecules in the first monolayer. Whereas the monolayer structure is largely determined by the molecule−substrate interactions, the second layer structure is expected to be dominated by molecule−molecule interactions.

The molecule−molecule interaction between a molecule in the second layer and the molecules in the first layer has been modeled by using a Lennard-Jones potential for the nonbonded carbon−carbon, carbon−hydrogen, and hydrogen−hydrogen interactions, as described in a previous report.[17] This allows an exploration of the potential landscape for different adsorption positions. The first monolayer is modeled with a cluster of 7 or 8 molecules for the hexagonal structure and the double-row structure, respectively. Figure 9 shows the molecule cluster and the results for the double-row structure. The interaction potential is calculated as a function of the adsorption height *z* and the *xy*-offset with respect to the molecule at the center of the cluster. We find adsorption energies of 1.6 eV per molecule in the second layer and a corresponding equilibrium distance of 3.35 Å. By varying the lateral offset of the second layer molecule we find the minimum energy at a small offset of ∼1.4 Å along the *x*-axis with respect to the molecule at the center of the monolayer cluster. The modulation with a periodicity of 2.5 Å originates from the preferred *ABA* stacking of graphene sheets and is responsible for the off-center position of the energy minimum. However, larger offsets are energetically unfavorable as seen by the adsorption energy at a bridge site of the monolayer molecules, which is lowered by ∼0.2 eV compared to the energy minimum near the on-top site. This mechanism is responsible for the transfer of structural information into the second monolayer and explains the experimentally observed double-row configuration in the second layer.

A fundamental difference between the first and the second monolayer is the formation of islands, which is observed in the second monolayer but is completely suppressed in the first monolayer. This shows that the molecule−molecule interaction is significantly modified by the substrate. From the Lennard-Jones modeling we find an attractive NN interaction of ∼0.08 eV. A possible origin of this substrate-mediated compensation of the attractive interaction is a molecule-induced redistribution of the local density of states at the surface. Such effects have been reported for other aromatic compounds adsorbed on Cu surfaces.[22,23]

Common Features of Investigated Molecules. The self-ordering of all molecules presented here is largely influenced by a prominent substrate−molecule interaction. This leads to a restriction on possible molecular orientations in the way that molecules are only adsorbed with carbon rings aligned with the close-packed Cu atom rows. Furthermore, the molecule−substrate interaction also determines the nearest-neighbor separation of the molecules, allowing only distances that are translationally equivalent with respect to the substrate lattice. However, it should be noted that this checkerboard behavior is not generally observed for monolayer structures of PAHs but rather depends on the molecular size and the geometrical shape of the molecular periphery as has been shown for monolayer structures of HBC and the rhombus-shaped $C_{54}H_{22}$ on GeS.[24,25] Accordingly, the monolayer structures depend on the subtle interplay of molecule−substrate and molecule−molecule interactions. The monolayer structures of PAHs on Cu(111) presented here are largely dominated by the molecule−substrate interaction and no structural units are observed which could be related to a specific attractive molecule−molecule interaction. More specifically, the monolayer structures are the densest possible commensurate arrangements of molecules that are allowed by steric repulsion between neighboring molecules.

Conclusion

We presented STM results on the self-ordering of HBC and two molecules with a slightly different structure, DBPP and DPO, on Cu(111). STM images of the different molecules allow a clear determination of the monolayer structure in view of the superstructure and the molecular orientation at the surface. The self-ordering into commensurate structures and the restriction on observed molecular orientations with carbon rings aligned with atom rows of the substrate evidences a checkerboard role of the substrate, and hence a dominant molecule−substrate interaction for all three planar PAHs investigated here. For DBPP we could show that the molecule position and orientation of the first layer are transmitted to the second layer by molecule−molecule interaction.

The fact that no attractive interaction exists for these PAH's on Cu(111) opens the possibility to introduce functional groups that lead to specific noncovalent bonds to either similar molecules or a second molecular species with high selectivity.

Acknowledgment. This work has been supported by the European commission within the STREP poject RADSAS and the Swiss Science Foundation (NCCR on Nanoscale Science).

Supporting Information Available: Synthesis concept and characterization of DPO. This material is available free of charge via the Internet at http://pubs.acs.org.

References and Notes

(1) Whitesides, G. M.; Grzybowski, B. *Science* **2002**, *295*, 2418.

(2) Yokoyama, T.; Yokoyama, S.; Kamikado, T.; Okuno, Y.; Mashiko, S. *Nature* **2001**, *413*, 619.
(3) Brune, H.; Giovannini, M.; Bromann, K.; Kern, K. *Nature* **1998**, *394*, 451.
(4) Brune, H. *Surf. Sci. Rep.* **1998**, *31*, 121.
(5) Corso, M.; Auwärter, W.; Muntwiler, M.; Tamai, A.; Greber, T.; Osterwalder, J. *Science* **2004**, *303*, 217.
(6) Rousset, S.; Repain, V.; Baudot, G.; Garreau, Y.; Lecoeur, J. *J. Phys.*: *Condens. Matter* **2003**, *15*, S3363.
(7) Theobald, J. A.; Oxtoby, N. S.; Philips, M. A.; Champness, N. R.; Beton, P. H. *Nature* **2003**, *424*, 1029.
(8) Barth, J. V.; Weckesser, J.; Cai, C.; Günter, P.; Bürgi, L.; Jeandupeux, O.; Kern, K. *Angew. Chem., Int. Ed.* **2000**, *39*, 1230.
(9) Lin, N.; Dmitriev, A.; Spillmann, H.; Messina, P.; Lingenfelder, M.; Stepanow, S.; Barth, J. V.; Kern, K. 12th International Conference on Scanning Tunneling Microscopy/Spectroscopy and Related Techniques. *AIP Conf. Proc.* **2003**, *696*, 144.
(10) Samori, P.; Severin, N.; Simpson, C. D.; Müllen, K.; Rabe, J. *J. Am. Chem. Soc.* **2002**, *124*, 9454.
(11) Jäckel, F.; Watson, M. D.; Müllen, K.; Rabe, J. P. *Phys. Rev. Lett.* **2004**, *92*, 188303.
(12) Florio, G. M.; Werblowsky, T. L.; Müller, T.; Berne, B. J.; Flynn, G. W. *J. Phys. Chem. B* **2005**, *109*, 4520.
(13) Lackinger, M.; Griessl, S.; Heckl, W. M.; Hietschold, M. *Anal. Bioanal. Chem.* **2002**, *374*, 685.
(14) Lackinger, M.; Müller, T.; Gopakumar, T. G.; Müller, F.; Hietschold, M.; Flynn, G. W. *J. Phys. Chem. B* **2004**, *108*, 2279.
(15) Herwig, P.; Kayser, C. W.; Müllen, K.; Spiess, H. W. *Adv. Mater.* **1996**, *8*, 510.
(16) de Craats, A. V.; Warman, J.; Fechtenkötters, A.; Brandt, J. D.; Müllen, K.; *Adv. Mater.* **1999**, *11*, 1469.
(17) Ruffieux, P.; Gröning, O.; Bielmann, M.; Simpson, C.; Müllen, K.; Schlapbach, L.; Gröning, P. *Phys. Rev. B* **2002**, *66*, 073409.
(18) Omicron Nanotechnology GmbH, D.-Taunusstein.
(19) Iyer, V. S.; Wehmeier, M.; Brand, J. D.; Keegstra, M. A.; Müllen, K. *Angew. Chem.* **1997**, *109*, 1675.
(20) Kübel, C.; Eckhardt, K.; Enkelmann, V.; Wegner, G.; Müllen, K. *J. Mater. Chem.* **2000**, *10*, 879.
(21) Gross, L.; Moresco, F.; Ruffieux, P.; Gourdon, A.; Joachim, C.; Rieder, K.-H. *Phys. Rev. B* **2005**, *71*, 165428.
(22) Lukas, S.; Witte, G.; Wöll, Ch. *Phys. Rev. Lett.* **2002**, *88*, 028301.
(23) Gross, L.; Moresco, F.; Savio, L.; Gourdon, A.; Joachim, C.; Rieder, K.-H. *Phys. Rev. Lett.* **2004**, *93*, 056103.
(24) Karl, N.; Günther, Ch. *Cryst. Res. Technol.* **1999**, *34*, 243.
(25) Günther, Ch.; Karl, N.; Pflaum, J.; Strohmaier, R.; Gompf, B.; Eisenmenger, W.; Müller, M.; Müllen, K. *Langmuir* **2005**, *21*, 656.